CHAPTER 7

MICRORHEOLOGY OF MECHANOSENSITIVE BONE CELLS

Rommel G. Bacabac[1], Daisuke S. Mizuno[2], Theo H. Smit[3], Jack J.W.A. Van Loon[1,4], Christoph Schmidt[2], Fred MacKintosh[5], Jenneke Klein-Nulend[1]

[1]Department of Oral Cell Biology, Academic Centre for Dentistry Amsterdam-Universiteit van Amsterdam and Vrije Universiteit, Amsterdam, The Netherlands
[2]Department of Physics of Complex Systems, Vrije Universiteit, Amsterdam, The Netherlands
[3]Department of Clinical Physics and Informatics, VU University Medical Center, Amsterdam, The Netherlands
[4]Dutch Experiment Support Center, Vrije Universiteit, Amsterdam, The Netherlands
[5]Department of Theoretical Physics, Vrije Universiteit, Amsterdam, The Netherlands

ABSTRACT

To understand how the mechanosensing by bone cells might relate to cellular metabolism and mechanical properties, a physical portrait of cell viscoelasticity is needed. Thus, we developed a novel application of two-particle microrheology using fibronectin-coated spherical probes to characterize the viscoelasticity, mechanically stimulate, and probe the mechano-activity of various cell types. We found that the elastic modulus of MLO-Y4 osteocytes was below 500 Pa, as well as for MC3T3-E1 osteoblasts, and primary osteocytes and osteoblasts. Interestingly, the nitric oxide released by MLO-Y4 cells increased after a mechanical stimulation at 5 pN, with cell-attached integrin-bound probes. This suggests that bone cells respond to forces at a similar range as for deforming integrins. MLO-Y4 cells interacted with the integrin-bound probes by changing their shape from spherical to being polar at $37^{o}C$. However, the same shape change at $22^{o}C$ was acquired by stimulation with 5-20 pN forces. This suggests that temperature has a significant effect on cell morphology. To probe the mechano-activity of bone cells, we measured the fluctuation of force $<ff^*>$ induced by the cells on the integrin-bound probes. $<ff^*>$ induced by MLO-Y4 cells were proportional to ω^{-2} (where frequency = $\omega/(2\pi)$) at frequencies < 3 Hz at $22^{o}C$. However, the force fluctuation was proportional to ω^{-2} for frequencies < 10 Hz at $37^{o}C$. Thus, temperature change possibly induces a sharp non-linear metabolic increase underlining the significant effect of the mechanical environment to cellular metabolism. Compared to MLO-Y4 cells, CCL-224 fibroblasts had a higher $<ff^*>$ magnitude at $37^{o}C$, as might be expected considering the motility of fibroblastic cells. The linear relation of $<ff^*>$ with ω^{-2} is a signature expected for continuums with slowly evolving internal processes. Hence, microrheology is a useful tool for understanding the varied set of observations on mechanosensing by bone cells and its implications on the osteogenic response of bone to mechanical loading.

INTRODUCTION

Cellular activity in response to stress stimuli has long been recognized. Previous reports have shown that cells respond to near zero gravity, fluid shear stress, strain stimuli, and vibration stress (1-4). Activation by mechanical loading has been shown to trigger chemical cascades that have significant roles for the metabolic maintainance of a global tissue to which the cell belongs. Mechanosensing, is the ability of cells to perceive forces, which includes the activity of different types of cells for transducing sound, for example, or for relaxing blood vessels at high fluid shear stress (5-7). The stress response of bone cells that direct osteogenic adaptation of bone to mechanical loading is an obvious example where mechanosensing by cells direct local changes that govern a global adaptation of the overall tissue. In bone, osteocytes are generally believed to sense the strain-induced fluid flow in the lacuno-canalicular system. In response to stress, osteocytes produce signaling molecules, e.g., nitric oxide (NO) and prostaglandin E_2 (PGE$_2$), that regulate the activity of other cells for building or resorbing bone (8-10).

The cytoskeleton of the cell has been acknowledged as one of the key factors in mechanosensing (11). The cytoskeleton is crucial for various cellular mechanisms, including the internal transport of vesicles (12), motility (13), and the fundamental support of cell shape. To understand the underlying mechanisms for the metabolic responses of cells to mechanical stress, a physical portrait of the viscoelastic properties of the cell is needed. Recent techniques in microrheology might prove crucial for probing the viscoelasticity of cells and its relevance to mechanosensing. For instance, the two-particle microrheology technique has been extended for characterizing inter-cellular force generators (14, 15).

In vitro, cells attach to substrates via focal adhesion centers for anchorage (16). Interestingly, some cells adapt to environmental stress by inducing contractile forces in relation to the stiffness of surrounding material (17). By induction of traction forces, possibly at focal adhesion centers, cells match

environmental stress and adapt morphology accordingly. Thus, mechanically-induced adaptation might be as important as chemically-mediated metabolic cascades. By probing changes in mechanical properties of cells, we might be able to understand mechanisms of cellular interaction with its stress environment.

Mechanical properties of soft materials, such as cells, can be studied by using techniques from microrheology. The two general approaches in microrheology pertain to the measurement of probe particle displacements embedded in the material investigated. The approach is either by inducing external forces on the probes (active mode) or by monitoring the thermal fluctuations of the probes (passive mode). Materials in thermal equilibrium are subject to a measurement of the complex shear modulus (G^*) due to the Fluctuation-dissipation theorem (18). For our purpose in this study, the cell is taken as a non-thermal system, that is, a complex material that is able by itself to induce forces while interacting with its environment. Recently, using intracellular probes, it was shown that cells exhibit internally slow evolving processes characterized by ω^{-2} power-law for internal force fluctuation (14, 19). Cells also show enhanced diffusion scaling as $t^{3/2}$ at short times by SV80 fibroblasts, of phagocytized or endogenous particles demonstrating the non-thermal activity of cells (12).

Paradigms taken for understanding cellular activation might include models for the mechanical properties of the cytoplasm as predominantly a continuum (20) or as composed of linked polymers that transfer forces through the cytoskeleton to the nucleus (11). A model linking cellular deformation to a chemical response by cells, might explain the significance of interconnectivity between the extra-cellular matrix, trans-membrane proteins and the cytoskeleton as a direct link to the cell nucleus (11, 21). An initial activation might involve the stretching of a protein, thereby exposing a cryptic section of the unfolded protein that reacts to immediately trigger a biochemical cascade (21). Thus, a continuous force transfer from the site of mechanical stimulation to the nucleus is not necessary. Regardless of the actual mechanisms that

induce a meaningful biochemical cascade, the mechanical property of the cell is important for mechanosensing since the mechanical property determines how the cell will deform.

The aim of this study is to investigate events occurring at the onset of mechanical stimulation. Thus, we developed here a two-particle assay for measuring the viscoelastic properties of cells and characterizing the chemical and mechanical activation of cells in response to stress. We extended the Hertz model for the deformation of an elastic (and viscoelastic) sphere upon the indentation of a rigid spherical probe to measure the elastic (and viscoelastic) response of a cell. Using the same two-particle assay, we measured nitric oxide release as a parameter for bone cell mechanosensitivity in response to sinusoidal forces. The mechanoactivity of bone cells was studied by measuring the morphological changes while being attached to the probe particles, and the force traction induced by the cells on the probes. Finally, the mechanoactivity of bone cells was characterized by inferring the fluctuation of the induced force traction of the cells on the probes.

MATERIALS AND METHODS

The elastic modulus of MLO-Y4, MC3T3-E1, primary osteocytes and osteoblasts, were measured at 22°C, using a two-particle assay for microrheology by attaching fibronectin-coated beads at opposite ends of the cells using an optical trap setup (bead attachment diagram shown in fig 1). The cell was deformed by sinusoidal movements of one of the attached beads, and the elastic modulus was determined as described in the section "Hertz model extended for viscoelastic spheres".

The elastic modulus of an MLO-Y4 cell, as a function of indentation depth, was measured at 22°C using an atomic force microscope (AFM) with a bead attached to the cantilever tip of the AFM using the Hertz model for round cells (for an application on thin regions of fibroblasts see (22)). The AFM

measurement was performed for a round MLO-Y4 cell that was partially attached to the substrate.

Nitric oxide released by MLO-Y4 cells was measured at 22$^\text{o}$C. Morphological changes of bone cells, as well as the force traction induced by cells on the attached beads, were measured at 37$^\text{o}$C. The apparent compliance measured by active and passive modes, at 22$^\text{o}$C, was compared for MLO-Y4 cells to illustrate the difference between the active and passive mode measurements. The apparent compliance of MLO-Y4, MC3T3-E1, primary osteocytes and osteoblasts, were measured at 22$^\text{o}$C and characterized by the force fluctuation. The force fluctuation of MLO-Y4 osteocytes was compared to that of CCL-224 fibroblasts at 37$^\text{o}$C.
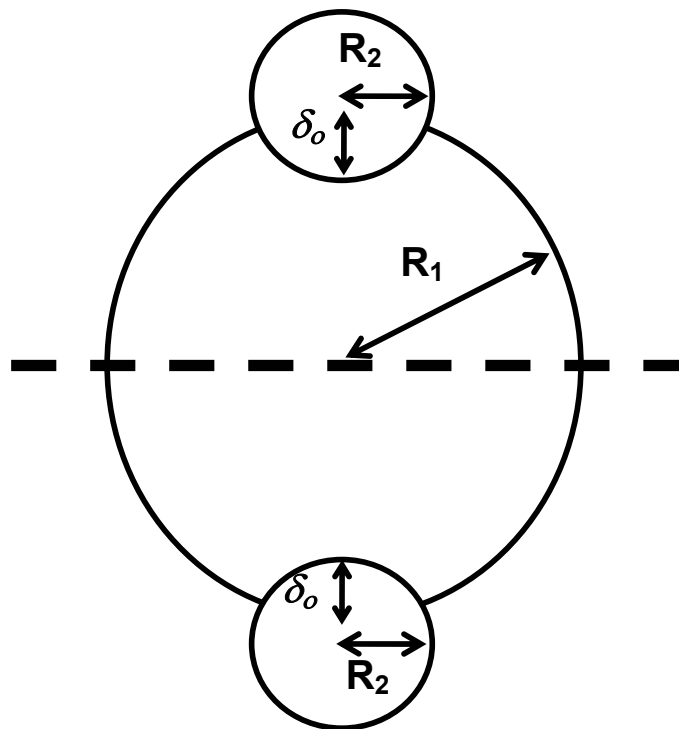

Figure 1. Hertz model for viscoelastic sphere indented with rigid spheres. Dashed line indicates the symmetry of the model.

Cell cultures

MLO-Y4 osteocytes were cultured at 37°C, up to near-confluency in 75 cm^2 cell culture flasks (Nunc, Roskilde, Denmark), using α-Modified Eagle's Medium (α-MEM; Gibco, Paisley, UK) supplemented with 5% fetal bovine serum (FBS; Gibco), 5% calf serum (CS; Gibco), penicillin (10μg/ml) and streptomycin (10μg/ml). The MLO-Y4 osteocytes were kindly provided by Dr. L. Bonewald (University of Missouri-Kansas City, Kansas City, MO, USA).

MC3T3-E1 cells were cultured at 37°C, up to near-confluency in 75 cm^2 cell culture flasks (Nunc), using α-MEM supplemented with 10% FBS, ascorbate (50 μg/ml; Merck, Darmstadt, Germany), β-glycerophosphate disodium salt hydrate (10 mM; Sigma, St. Louis, MO, USA), l-glutamine (300 μg/ml; Merck), gentamycine (50 μg/ml; Gibco), and fungizone (1.25 μg/ml; Gibco). The MC3T3-E1 osteoblasts were kindly provided by Dr. M. Kumegawa (Meikai University, Sakado, Japan).

CCL-224 fibroblasts were cultured at 37°C, up to near-confluency using α-MEM supplemented with 10% FBS, penicillin (10μg/ml) and streptomycin (10μg/ml). The CCL-224 cells were kindly provided by Dr. J. Boonstra, (Utrecht University, Utrecht, the Netherlands).

MLO-Y4, MC3T3-E1, and CCL-224 cells were harvested by 10 min treatment with 0.05% trypsin/0.01% EDTA in PBS at 37°C. These cells were incubated in ice-water water bath after harvesting. Prior to experiments, these cells were equilibrated to 22°C or 37°C in CO_2-independent medium (Gibco) without supplements.

Primary bone cell isolations

Fetal chicken calvarial cells were isolated as described by Ajubi *et al.* (23). Calvariae were aseptically dissected from 18-day-old chicken fetuses. A mixed population of osteocytes and osteoblasts was obtained from the calvariae by sequential treatments of 1 mg/ml collagenase (Sigma, St. Louis, MO, USA)

and 4 mM EDTA. Osteocytes were identified from the mixed population of cells using a specific anti-body OB 7.3 directed to antigens on the cytoplasmic membrane (24). Using an immunodissection method based on Van der Plas and Nijweide, 1992 (25), osteocytes were isolated and purified from the mixed cell population of osteocytes and osteoblasts. After isolation, Osteocytes and osteoblasts were cultured separately in 75 cm^2 cell culture flasks (Nunc) with α-MEM, containing 2% chicken serum (Gibco), 200 μg/ml glutamine (Sigma), 50 μg/ml gentamycin sulfate (Sigma), 50 μg/ml L-ascorbic acid (BDH, Brunschwig Chemie, Amsterdam, The Netherlands), and 1 mg/ml D-glucose. After one day, the osteocytes and osteoblasts were harvested by 5 min treatment with 0.05% trypsin/0.01% EDTA in PBS at 37°C. These cells were incubated in ice-water water bath after harvesting. Prior to experiments, these cells were equilibrated to 22°C or 37°C in CO$_2$-independent medium (Gibco) without supplements.

DAR4M loading for nitric oxide fluorescence

For nitric oxide determination, MLO-Y4 cells were treated with a membrane-permeable fluorescent indicator Diaminorhodamine-4M AM (DAR-4M AM; Daiichi Pure Chemicals, Tokyo, Japan) (26). The intracellular DAR-4M AM treatment of cells lasted for 1 hr while the cells were incubated in ice-water bath. Prior to experiments, the cells were equilibrated to 22°C in CO$_2$-independent medium (Gibco) without supplements. To test whether an increase of fluorescence signal is induced by the presence of NO, 20 mM of the NO donor S-nitroso-N-acetylpenicillamine (SNAP; Sigma) was added to MLO-Y4 cells treated with DAR-4M AM.

Preparation of fibronectin-coated microspheres (beads)

Carboxyl-modified 4 μm diameter-polystyrene microspheres (beads; Bangs Laboratories, Inc., Fishers, IN, USA) were cleaned and coated with fibronectin

(Gibco) according to the manufacturer's instructions (Bangs Laboratories, Inc.). The fibronectin-coated beads were suspended in phosphate buffered saline (PBS; Gibco) with 0.1% bovine serum albumin (BSA; Gibco). For the experiments, the fibronectin-coated beads were cleaned with PBS and sonicated for 5 min to remove aggregations. The beads were then re-suspended in CO_2-independent medium and equilibrated to $22^{\circ}C$ or $37^{\circ}C$.

Preparation of dichloro-dimethyl-silane coated cover slips

24 x 50 mm cover slips (Menzel-Glaser, Braunschweig, Germany) used as the bottom surface of the culture chamber for observation in the optical trap setup were made hydrophobic by coating them with dichloro-dimethyl-silane (DDS; Acros Organics, USA). The cover slips were sequentially treated with KOH (30 g/200 ml ethanol) for 30 min and sequentially rinsed in distilled water (3 s), HCl (5% in distilled water for 3 s), and ethanol (3 s). After completely drying the cover slips, they were treated with DDS in trichloroethylene (TCE; Acros Organics, Morris Plains, NJ, USA) for 5 min. The treated cover slips were rinsed with ethanol for 2-5 min under sonic bath before overnight annealing at $80^{\circ}C$.

Preparation of Atomic force microscope cantilever

12 μm diameter-polystyrene microspheres (beads; Bangs Laboratories, Inc.) were attached to an atomic force microscope cantilever (stiffness 0.05 N/m, resonance frequency 18 kHz). The cantilever was cleaned with toluene and acetone. The cantilever tip was then treated with ultraviolet-hardened glue (UV-glue, 1 part in 5 parts toluene), and was left to dry. The treated cantilever was attached to a micropipette tip at the end opposite the tip, with grease. The cantilever was subsequently immersed in a suspension of beads. After a bead was conveniently located at the cantilever tip, it was irradiated with UV to permanently attach the bead to the cantilever tip.

Hertz model extended for viscoelastic spheres

To measure cell viscoelasticity, we extended the Hertz model (reference Hertz) for viscoelastic spheres. The force-indentation relation for contact between two elastic spheres has been described by Timoshenko and Goodier (27). Here we extend this model for a rigid spherical probe indenting a viscoelastic sphere, the force F is related to a 3/2 scaling-law due to the indentation depth d:

$$F = \frac{4}{3}\sqrt{\frac{R_1 R_2}{R_1 + R_2}}\left(\frac{E_o}{1-\nu^2}d^{3/2}\right)$$ [1]

where R_1 and R_2, are the radii of the cell and the probe (fig 1), the homogenous elastic modulus E_o and the Poisson ratio ν. Since we attach the probe to the cell, we induce a constant indentation depth of d_o and perturb about this value sinusoidally at amplitude d. By a Taylor expansion about d_o, we find a complex modulus E^*:

$$F = \frac{4}{3}\sqrt{\frac{R_1 R_2}{R_1 + R_2}}\left(\frac{E_o}{1-\nu^2}d_o^{3/2} + \frac{3E^*}{2(1-\nu^2)}\sqrt{d_o}d\right)$$ [2]

where E_o is an elastic contribution due to a constant force F_o (see also Mahaffy et al. for an application for flat cells using "atomic force microscopy" or AFM (22)). By setting F_o to zero, i.e., by assuring that the applied force oscillates about zero, the complex modulus E^* is found as follows:

$$F = F_o + F^*$$ [3]

setting $F_o = 0$, the applied force F^* becomes linear with the indentation d (provided $d < d_o$):

$$F^* = 2\sqrt{\frac{R_1 R_2}{R_1 + R_2}}\left(\frac{E^*}{1-\nu^2}\right)\left(\sqrt{d_o}\right)d$$ [4]

Hence, the complex modulus is:

$$E^* = E' + iE''$$ [5a]

where the loss and storage moduli are E' and E'', respectively. The elastic modulus is then calculated as $|E^*|/(1-\nu^2)$ or simply $E/(1-\nu^2)$:

$$\frac{|E^*|}{(1-\nu^2)} = \frac{E}{(1-\nu^2)} = \frac{|F^*|}{2d}\sqrt{\frac{R_1 + R_2}{R_1 R_2 d_o}}$$ [5b]

which is related to the shear modulus:

$$|G*| = \frac{E}{2(1+v)} \qquad [5c]$$

The cell stiffness k_{12} is related to the trap stiffnesses, k_1 and k_2, in our two-particle assay, constituting a three-spring series (fig 2). The force-balance equations, with the forces at the probes, f_1 and f_2, the displacements of the beads x_1 and x_2, and the stiffnesses, are as follows:

$$\begin{pmatrix} f_1 \\ f_2 \end{pmatrix} = \begin{pmatrix} k_1 + k_2 & -k_{12} \\ -k_{12} & k_2 + k_{12} \end{pmatrix} \begin{pmatrix} x_1 \\ x_2 \end{pmatrix} \qquad [6]$$

Hence the apparent compliance A_{ij} (mutual compliance for $i \neq j$) is simply the inverse of the stiffness matrix k_{ij} above, at the quasi-steady regime:

$$\begin{pmatrix} x_1 \\ x_2 \end{pmatrix} = \begin{pmatrix} A_{11} & A_{12} \\ A_{21} & A_{22} \end{pmatrix} \begin{pmatrix} f_1 \\ f_2 \end{pmatrix} \qquad [7a]$$

$$\begin{pmatrix} A_{11} & A_{12} \\ A_{21} & A_{22} \end{pmatrix} = \frac{1}{(k_1 + k_{12})(k_2 + k_{12}) - (k_{12})^2} \begin{pmatrix} k_1 + k_{12} & k_{12} \\ k_{12} & k_2 + k_{12} \end{pmatrix} \qquad [7b]$$

The apparent compliance was measured in the active mode directly from the movement of the particles at 0.1 Hz and 0.5 Hz. At higher frequencies, we used a lock-in amplifier technique referenced from the frequency at the acousto-optical device in the optical trap setup (see fig 3 for a diagram of the setup).
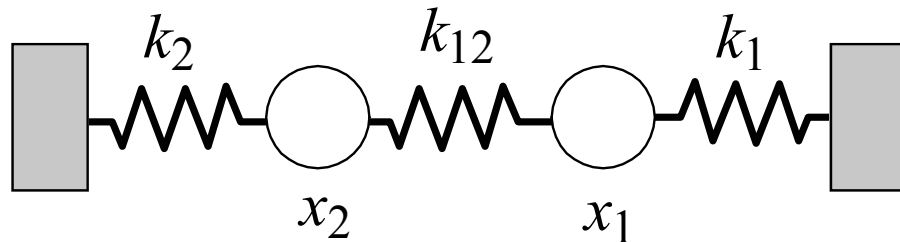

Figure 2. Spring series model for two-particle microrheology assay for cells. k_1, k_2 are optical trap stiffnesses; k_{12}, cell stiffness; x_1 and x_2, particle displacements.

Passive microrheology

By observing the fluctuations of each probe and the mutual fluctuations of the beads, the complex compliances are calculated from the auto-correlations and cross-correlations of the particles. Details of the techniques for both one and two-particle microrheogy has been described previously (15, 28, 29). Based on the fluctuation-dissipation theorem, the imaginary component of the compliance α_{ij}" (mutual apparent compliances where $i \neq j$) is related to the thermal energy $k_B T$ as follows:

$$\langle x_i(\omega)x_j(\omega) \rangle = 4k_B T \alpha_{ij}"(\omega)/\omega \quad i = 1,2 \tag{8}$$

where, k_B is the Boltzmann constant, T is the absolute temperature, and the frequency $= \omega/(2\pi)$. The Kramers-Kronig relation is used to find the real component of the apparent compliance α_{ij}':

$$\alpha_{ij}'(\omega) = \frac{2}{\pi} P \int_0^\infty \frac{\chi \alpha_{ij}"}{\chi^2 - \omega^2} d\chi \quad i,j = 1,2 \tag{9}$$

For the quasi-steady regimes, the cell compliance α_{12} is calculated by setting $1/k_{12} = \alpha_{12}$ in [7]. The components of the complex compliance of the cell α_{12} are linear to the corresponding components of the apparent compliance A_{12}:

$$\alpha_{12} = \alpha' + i\alpha" \tag{10a}$$

$$\alpha_{12} = \left(\frac{A_{12}'}{|A_{12}*|^2 k_1 k_2} - \frac{k_1 + k_2}{k_1 k_2} \right) + i\left(\frac{-A_{12}"}{|A_{12}*|^2 k_1 k_2} \right) \tag{10b}$$
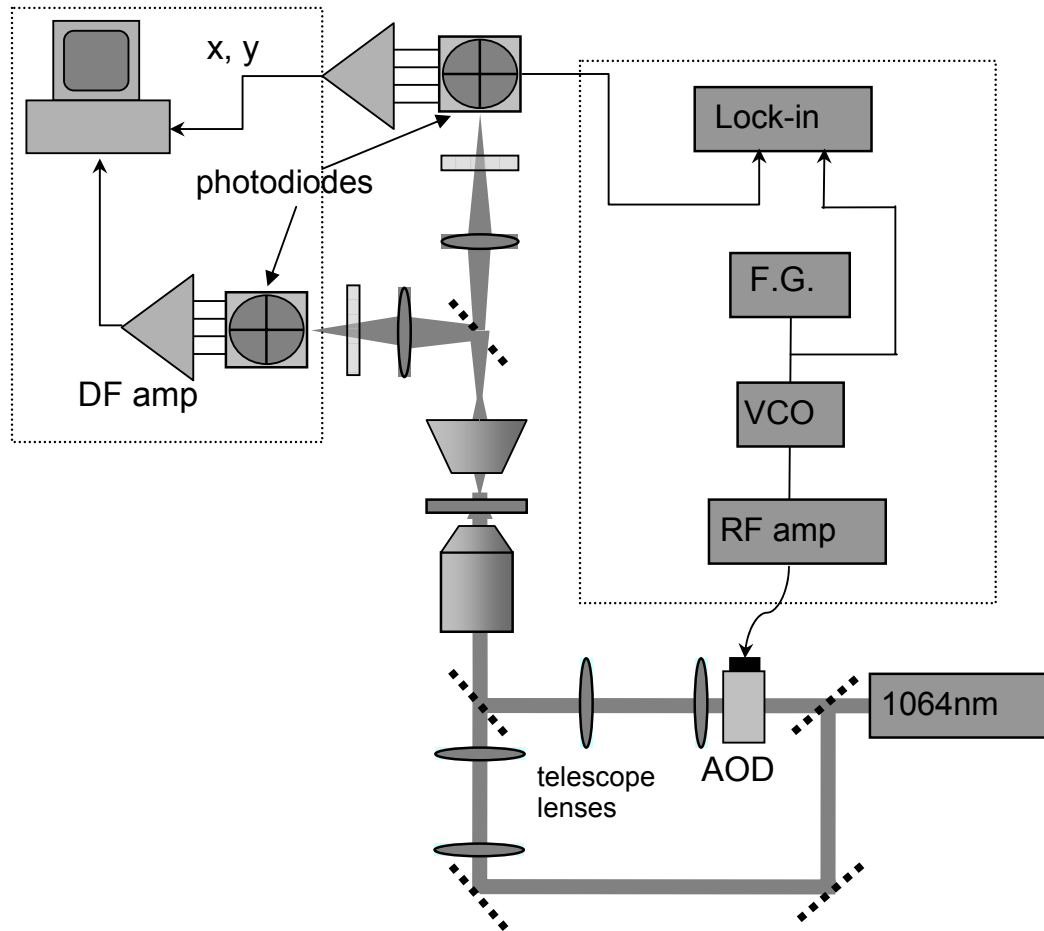
Figure 3. Schematic diagram of experimental setup. 1064 nm laser beam is diverted in two paths for trapping two particles. One of the beams is manipulated by using an acoustic optical device (AOD). A lock-in amplifier is used for measurements of the frequency response. DF amp, differential amplifier; F.G., function generator; VCO, voltage controlled oscillator; RF amp, radio frequency amplifier.

Non-thermal force fluctuation

A Generalized Langevin equation is used to model the force-balance in our two-particle assay for the microrheology of cells. The force on a small thermal particle with velocity u_i is related to a memory friction $\xi_{ij}(t)$ (mutual memory friction for $i \neq j$) of the complex material:

$$m_i \frac{du_i(t)}{dt} = f_{Ri}(t) - \int_{-\infty}^{t} \xi_{ij}(t-t')u_i(t')dt' \qquad \text{[11a]}$$

where f_{Ri} represents all forces acting on particle i, including an inter-particle force f_I (in this case, comprising non-thermal forces from the cell), forces from the laser traps with stiffness $k_i x_i$, and stochastic Brownian forces K_i:

$$f_{Ri} = -k_i x_i + K_i + f_I \qquad [11b]$$

Zero resultant force is expected in our two-particle assay, thus the coupled force-balance equations are:

$$\int_{-\infty}^{t} \xi_{11}(t-t') u_1(t') dt' = -\int_{-\infty}^{t} \xi_{12}(t-t') u_2(t') dt' - k_1 x_1 + K_1 + f \qquad [12a]$$

$$\int_{-\infty}^{t} \xi_{22}(t-t') u_2(t') dt' = -\int_{-\infty}^{t} \xi_{21}(t-t') u_2(t') dt' - k_2 x_2 + K_2 - f \qquad [12b]$$

Where the thermal force fluctuation is:

$$\left\langle K_i(t) K_j(t') \right\rangle = 2 k_B T \xi_{ij}(t-t') \qquad [13]$$

The non-thermal force fluctuation is then simply the difference between the total force fluctuation in the assay based on the displacement fluctuation of the probe particles $\langle x_1 \, x_2 {}^* \rangle$, and the thermal force fluctuation. The power spectrum of the non-thermal fluctuation $\langle x_1 x_2 {}^* \rangle$ is:

$$\left\langle x_1 x_2 {}^* \right\rangle - \frac{4 k_B T \alpha_{12}''}{\omega} = -\Delta(\omega)\left\{ (A_{11}'' - A_{12}'')^2 + (A_{11}' - A_{12}')^2 \right\} \qquad [13]$$

where $\Delta(\omega)$ represents the power spectrum of the fluctuation. Alternately, the force fluctuation is directly measured as:

$$\left\langle f(t) f(t') \right\rangle = 2 k_B T \Delta(t-t') \qquad [14]$$

with the power spectrum:

$$\left\langle f f {}^* \right\rangle = \frac{2 k_B T}{\sqrt{2\pi}} \Delta(\omega) \qquad [15]$$

RESULTS

The typical force-displacement curves for MLO-Y4 cells and primary osteocyte cells showed a linear relation between the applied force and the cell

diameter change (2d, fig 4A and B). This shows that our model is accurate for determining the elastic modulus of cells for the quasi-steady regime (here taken at 0.1 Hz). The elastic moduli ($E/(1-\nu^2)$) of the bone cells were all similarly below 1 kPa, except for one osteocyte cell, which had an elastic modulus about 1.4 kPa (fig 5A). The MLO-Y4 modulus varied between 35 Pa and 430 Pa (fig 5A). Using AFM with the Hertz model for round cells, the elastic modulus of a MLO-Y4 osteocyte was shown to vary from 65 Pa to 230 Pa, for indentation depths varying between 4800 to 7900 nm (fig 5B).

To investigate the effects of mechanical loading on cell using pN forces, the accumulated nitric oxide (NO) released by MLO-Y4 cells were monitored. A typical MLO-Y4 cell treated with DAR-4M-AM indicated continued fluorescence increase with the addition of 20 nM SNAP (data shown for 60 s, fig 6A). The effect of small changes in force amplitudes was investigated by stimulating MLO-Y4 cells with sinusoidal force at amplitudes 5, 7.5, 10, and 12.5 pN, all at 0.1 Hz (each regime taken at durations of 60s). Total fluorescence intensity increase was found simultaneous to force application at 0.1 Hz (fig 6B and C). Fluorescence intensity increased from the basal level upto 60 s as a force amplitude of 5pN was applied (fig 6B). An abrupt increase was observed when a force amplitude of 7.5 pN was applied (at about the 60 s time point); afterwards, the intensity was nearly stable beyond 200 s of force application. The sharp increase with the application of 10 pN force amplitude is attributed to a possible artifact by perturbation of the cell position disturbing the fluorescence intensity, as the intensity went back to the stable level (fig 6B). Simultaneous with the observation of fluorescence intensity increase, the cellular traction force was found to increase from 0 to 60 pN in the period of 4 min (fig 6 B). Another MLO-Y4 cell was stimulated with sinusoidal loading at 0.1 Hz with amplitudes 5, 10, 15 pN at one-min intervals. After 1 min of 5 pN stimulation, the fluorescence intensity increased from the basal level and remained stable (fig 6C). This increase occurred while the cell was stimulated with 10 pN sinusoidal force, and remained at a stable value despite further stimulation with 15 pN (fig 6C).
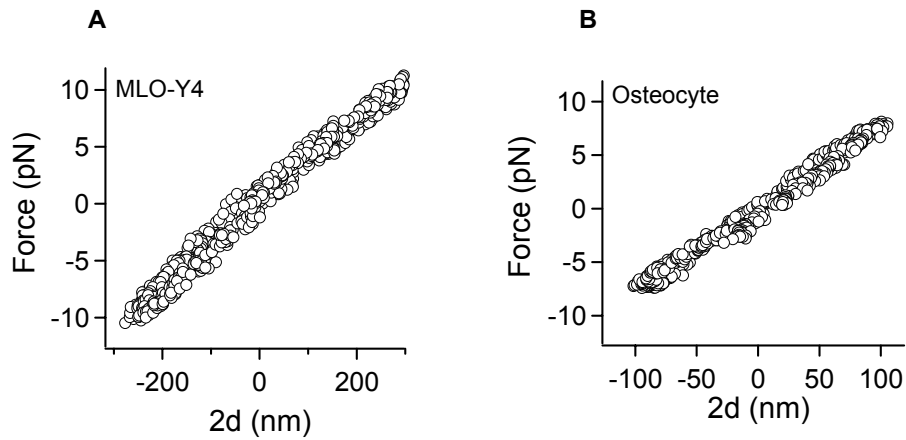
A

B

Figure 4. Force-displacement curves. A. MLO-Y4. B. Osteocyte. 2d, change in cell diameter.
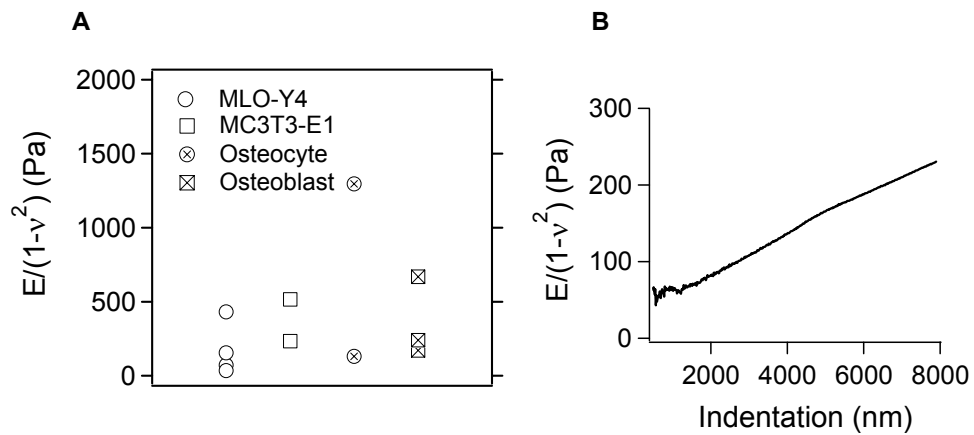
A

B

Figure 5. Elastic moduli E. A. Elastic moduli for bone cells. B. Elastic modulus change of a round MLO-Y4 cell in relation to indentation depth by atomic force microscopy.
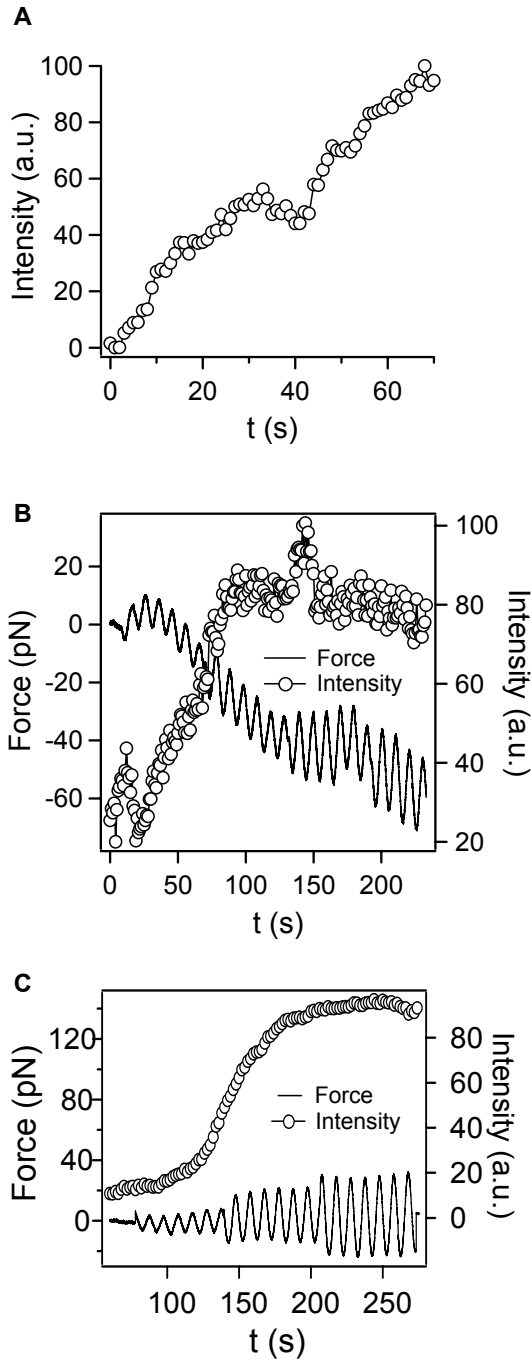
A

Figure 6. Nitric oxide release. A. Fluorescence intensity increase in MLO-Y4 cell treated with 20 mM SNAP solution. B. Nitric oxide release and MLO-Y4 cell induction of contractile force while stimulated with 0.1 Hz sinusoidal force with increasing amplitudes at 22°C. C. Nitric oxide release of MLO-Y4 cell while stimulated with sinusoidal force at 0.1 Hz, at increasing amplitudes.
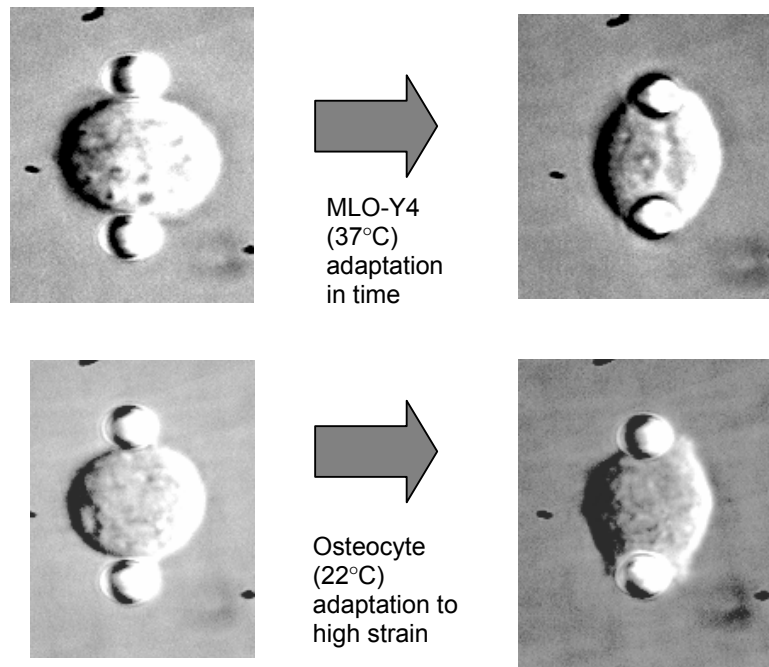
B

C

Figure 7. Morphology adaptation. A. MLO-Y4 cell changed morphology from spherical to polar shape at 37°C, without force stimulation. B. Osteocyte cell changed morphology from spherical to polar shape at 22°C, after stimulation with sinusoidal force at 0.1 Hz, with increasing amplitudes from 5pN to nearly 30pN.

MLO-Y4 cells, while attached to two particles, showed morphological adaptation within ~ 20 min at 37°C (typical change shown in fig 7). The cell changed from a spherical to a polar shape at the attachment sites (fig 7). At 22°C, an osteocyte cell was subjected to sinusoidal forces at 0.1 Hz, at increasing amplitudes (between 5 to 20 pN). The tension was released after each sinusoidal force stimulation, every 30s. The osteocyte adapted by changing shape from spherical to being polar at the attachment sites (fig 7). At 37°C the contractile force of an MLO-Y4 cell on the attached particle was found to increase to 30 pN in 60s (fig 8A). For another MLO-Y4 cell, also at 37°C, the contractile force varied periodically and reached a peak at 30 pN in 30s (fig 8B). The contractile forces on the attached particles appeared to be

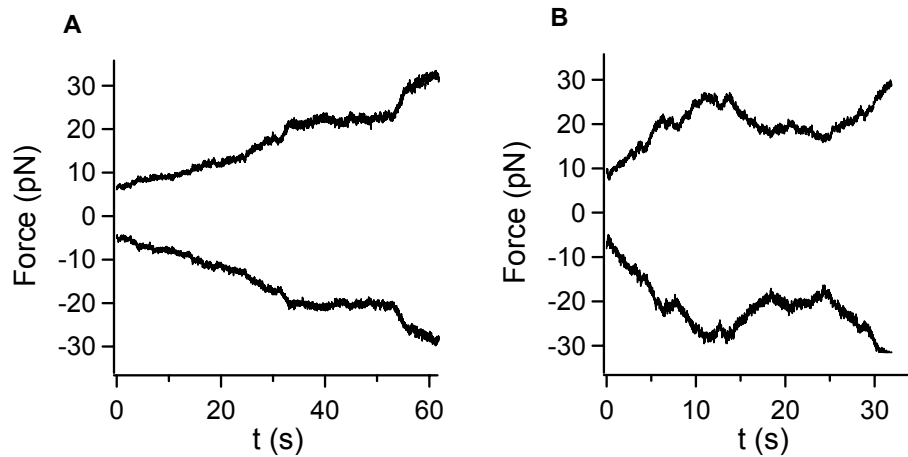consistently anti-correlating, as the experiment configuration is symmetric (fig 8A and B).

Figure 8. MLO-Y4 cell induction of contractile force. A. at 22°C. B. at 37°C.

The apparent compliance of osteocytes, and MLO-Y4 cells measured by active or passive modes were compared for measurements performed at 22°C and 37°C, respectively. At 22°C the real component of the apparent compliance, A_{12}' of osteocytes measured by active or passive modes was similar (fig 9A). However, the imaginary component of the apparent compliance, A_{12}'', measured by passive mode was negative and much lower compared to A_{12}'' measured by active mode until around 3 Hz (fig 9A). At 37°C A_{12}' measured by active and passive modes for MLO-Y4 cells, were similar in value, but A_{12}'' measured by active and passive modes differed (fig 9B). Whereas, A_{12}'' by active mode was nearly zero, A_{12}'' by passive mode was negative until about 10 Hz.

To compare the mechanical activity of different cell types, the force fluctuation $<ff^*>$, based on equation [15] was measured for MLO-Y4, MC3T3-E1 cells, primary osteocytes and primary osteoblasts at 22°C, and for MLO-Y4 and CCL-224 fibroblasts at 37°C. At 22°C, the force fluctuation for all cell-types was found proportional to ω^{-2} for frequencies ≤ 3 Hz (fig 10). The force fluctuation for MLO-Y4 cells were found higher than MC3T3-E1 cells (fig 10).

Also, osteocytes exhibited higher force fluctuation compared to osteoblasts (fig 10). The force fluctuation of MC3T3-E1 cells was found relatively similar to osteocytes (fig 10). At 37°C the force fluctuation of CCL-224 fibroblasts was a decade higher than MLO-Y4 cells (fig 11). However, the force fluctuation of both MLO-Y4 and CCL-224 cells were proportional to ω^{-2} for frequencies ≤ 10 Hz.
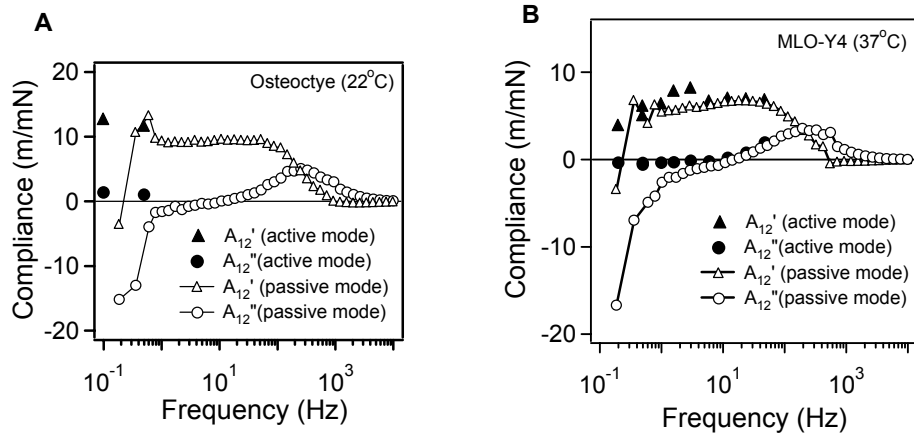

Figure 9. Apparent compliance. A. Osteocyte cell at 22°C. B. MLO-Y4 at 37°C
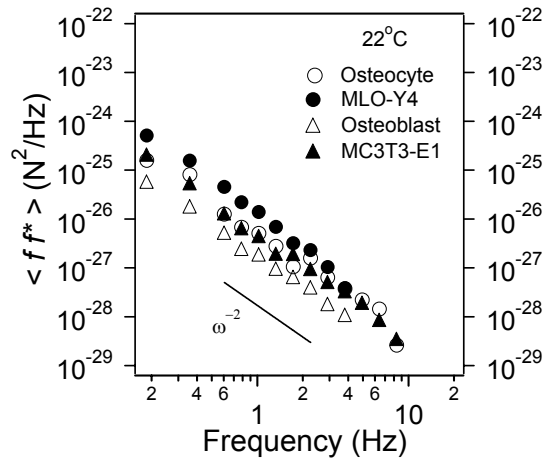

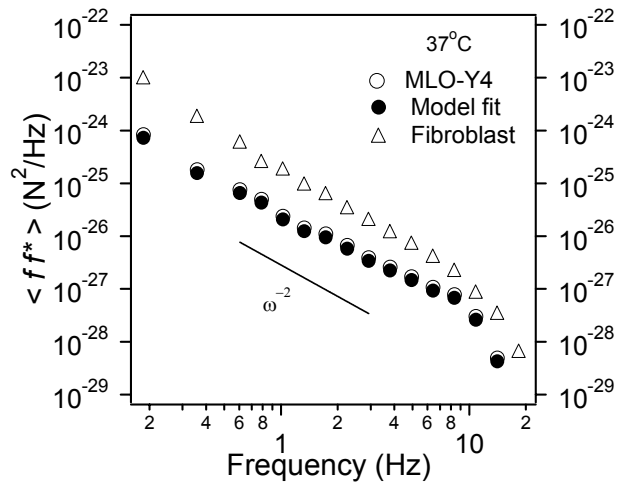**Figure 10.** Force fluctuation at 22°C by bone cells

Figure 11. Force fluctuation at 37°C by MLO-Y4 osteocytes and CCL-224 fibroblasts.

DISCUSSION

The elastic moduli of the bone cells were similarly below 1 kPa, except for one osteocyte with an elastic modulus nearly 1.4 kPa. The elastic modulus of MLO-Y4 cells, as measured by optical tweezers, were confirmed to be within a similar range of values, as measured by AFM on a round MLO-Y4 cell. However, the AFM results also showed that the elastic modulus of a round MLO-Y4 cell varied with increasing indentation depth by the AFM cantilever. Thus, the elastic modulus of a cell is strongly dependent to the applied stress. Previously, we showed that osteocytes are more mechanosensitive than osteoblasts (1). Since the elastic modulus of the different bone cell types were similar, this might indicate that differences in mechanosensitivity between cells might be more related to how cells change moduli in relation to deformation.

MLO-Y4 cells showed an increased release of NO (by increase in fluorescence intensity) after about 1 min mechanical stimulation of 5 pN. Simultaneous with increased NO release was the observed increased force traction on the attached bead. Continued morphological adaptation by MLO-Y4 cells during bead attachment, supports the notion that morphology and force induction by cells are related. Since, force traction is simultaneous with

morphological changes and morphological changes is directly related to the elasticity of the cell, the release of NO is possibly related to changes in the elastic modulus of the cell. Furthermore, we have shown that force traction of the cells increased up to nearly 30 pN, which is within the order of force values necessary for activating integrins (30, 31), which was interestingly within the order of the forces we used to stimulate NO release. Cells might adapt their elasticity in relation to their stress environment, in a strong relation to their physiological activity, *e.g.*, the release of a signaling molecule.

The apparent compliance is linear to the actual compliance as indicated in equation [10], provided, within negligible momentum effects due to the surrounding fluid. Our apparent compliance measurements, indicate that the MLO-Y4 cells change viscoelasticity in strong relation to temperature. Since A_{12}' is proportional to the cross-correlation of the fluctuations of the two attached beads, this difference measures the force traction of the cells below a cross-over frequency (3 Hz for 22°C, 10 Hz for 37°C). The cross-over frequency, separates the non-thermal activity (or cellular activity) from thermal activity. The differece between 22°C and 37°C is negligible (in the Kelvin scale). Hence, an order of difference between cross-over frequencies might indicate a non-linear transition due to temperature for the activity of cells. This further illustrates the importance of temperature for directing metabolic activities of the cell and the non-linear properties of cells. In general, the mechanical stress environment of a cell strongly influences its behavior.

The proportionality between the cellular force fluctuation with ω^{-2}, indicates a quantifiable signature for non-thermal related activity by bone cells. This signature is expected in continuums with slowly evolving internal processes (14). All cells in this study exhibited this signature. However, the magnitude of the force fluctuations $<ff^*>$ varied across cell types at 22°C and 37°C. It is interesting that this variation across cell types indicates that osteocytes have a higher mechanoactivity than osteoblasts. However, we also showed that the force fluctuation by CCL-224 is an order higher than that of osteocytes. This

supports the notion that fibroblasts have a high metabolism, which is necessary for motility.

The force fluctuation is indicative of internal metabolic processes. Our results have shown that osteocytes are also more mechanoactive compared to osteoblasts. However, fibroblasts, are even more mechanoactive than osteocytes. This, however, does not correlate with our earlier result showing that fibroblasts are least mechanosensitive compared to osteocytes and osteoblasts (32). Thus, mechanoactivity and mechanosensitivity, though related might not necessarily correlate.

In conclusion, we have shown the use of microrheology to probe the possible novel correlations between mechanosensitivity, mechano-activity, and the viscoelasticity of bone cells. Our results might prove useful for numerical models for cells in relation to their functional activity in bone. Techniques in microrheology provide quantifiable measures for explaining the varied set of observations in studying the response of bone cells to stress and its implications for the osteogenic response of bone to mechanical loading.

ACKNOWLEDGEMENTS

REFERENCES

1. Klein-Nulend J, van der Plas A, Semeins CM, Ajubi NE, Frangos JA, Nijweide PJ, Burger EH 1995 Sensitivity of osteocytes to biomechanical stress in vitro. FASEB J 9(5):441-445.

2. Owan I, Burr DB, Turner CH, Qiu J, Tu Y, Onyia JE, Duncan RL 1997 Mechanotransduction in bone: osteoblasts are more responsive to fluid forces than mechanical strain. Am J Physiol 273(3 Pt 1):C810-C815.

3. Judex S, Boyd S, Qin YX, Turner S, Ye K, Muller R, Rubin C 2003 Adaptations of trabecular bone to low magnitude vibrations result in more uniform stress and strain under load. Ann Biomed Eng 31(1):12-20.

4. Cogoli A, Tschopp A, Fuchsbislin P 1984 Cell Sensitivity to Gravity. Science 225(4658):228-230.

5. Haidekker MA, Stevens HY, Frangos JA 2004 Cell membrane fluidity changes and membrane undulations observed using a laser scattering technique. Ann Biomed Eng 32(4):531-536.

6. White CR, Haidekker M, Bao X, Frangos JA 2001 Temporal gradients in shear, but not spatial gradients, stimulate endothelial cell proliferation. Circulation 103(20):2508-2513.

7. Kros C 2005 Hearing: aid from hair force. Nature 433(7028):810-811.

8. Burger EH, Klein-Nulend J 1999 Mechanotransduction in bone - Role of the lacuno-canalicular network. FASEB J 13(Supplement):S101-S112.

9. Burger EH, Klein-Nulend J, Van der Plas A, Nijweide PJ 1995 Function of osteocytes in bone--their role in mechanotransduction. J Nutr 125(7 Suppl):2020S-2023S.

10. Klein-Nulend J, Semeins CM, Ajubi NE, Nijweide PJ, Burger EH 1995 Pulsating fluid flow increases nitric oxide (NO) synthesis by osteocytes but not periosteal fibroblasts--correlation with prostaglandin upregulation. Biochem Biophys Res Commun 217(2):640-648.

11. Wang N, Butler JP, Ingber DE 1993 Mechanotransduction across the cell surface and through the cytoskeleton. Science 260(5111):1124-1127.

12. Caspi A, Granek R, Elbaum M 2000 Enhanced diffusion in active intracellular transport. Phys Rev Lett 85(26):5655-5658.

13. Kole TP, Tseng Y, Jiang I, Katz JL, Wirtz D 2005 Intracellular mechanics of migrating fibroblasts. Mol Biol Cell 16(1):328-338.

14. Lau AW, Hoffman BD, Davies A, Crocker JC, Lubensky TC 2003 Microrheology, stress fluctuations, and active behavior of living cells. Phys Rev Lett 91(19):198101-1-198101-4.

15. Crocker JC, Valentine MT, Weeks ER, Gisler T, Kaplan PD, Yodh AG, Weitz DA 2000 Two-point microrheology of inhomogeneous soft materials. Phys Rev Lett 85(4):888-891.

16. Petit V, Thiery JP 2000 Focal adhesions: structure and dynamics. Biol Cell 92(7):477-494.

17. Pelham RJ, Wang YL 1997 Cell locomotion and focal adhesions are regulated by substrate flexibility. Proc Natl Acad Sci USA 94(25):13661-13665.

18. Chaikin PM, Lubensky TC 1995 Principles of condensed matter physics, Cambridge University Press, New York.

19. Fabry B, Maksym GN, Butler JP, Glogauer M, Navajas D, Fredberg JJ 2001 Scaling the microrheology of living cells. Phys Rev Lett 87(14):148102.

20. Karcher H, Lammerding J, Huang HD, Lee RT, Kamm RD, Kaazempur-Mofrad MR 2003 A three-dimensional viscoelastic model for cell deformation with experimental verification. Biophys J 85(5):3336-3349.

21. Janmey PA, Weitz DA 2004 Dealing with mechanics: mechanisms of force transduction in cells. Tren Biochem Sci 29(7):364-370.

22. Mahaffy RE, Park S, Gerde E, Kas J, Shih CK 2004 Quantitative analysis of the viscoelastic properties of thin regions of fibroblasts using atomic force microscopy. Biophys J 86(3):1777-1793.

23. Ajubi NE, Klein-Nulend J, Nijweide PJ, Vrijheid-Lammers T, Alblas MJ, Burger EH 1996 Pulsating fluid flow increases prostaglandin production by cultured chicken osteocytes--a cytoskeleton-dependent process. Biochem Biophys Res Commun 225(1):62-68.

24. Nijweide PJ, Mulder RJ 1986 Identification of osteocytes in osteoblast-like cell cultures using a monoclonal antibody specifically directed against osteocytes. Histochem 84(4-6):342-347.

25. van der PA, Nijweide PJ 1992 Isolation and purification of osteocytes. J Bone Miner Res 7(4):389-396.

26. Kojima H, Hirotani M, Nakatsubo N, Kikuchi K, Urano Y, Higuchi T, Hirata Y, Nagano T 2001 Bioimaging of nitric oxide with fluorescent indicators based on the rhodamine chromophore. Anal Chem 73(9):1967-1973.

27. Timoshenko SP, Goodier JN 1970 Theory of elasticity, 3rd ed, McGraw-Hill Book Company, Singapore.

28. Levine AJ, Lubensky TC 2000 One- and two-particle microrheology. Phys Rev Lett 85(8):1774-1777.

29. Levine AJ, Lubensky TC 2001 Response function of a sphere in a viscoelastic two-fluid medium. Phys Rev E 6304(4):041510-1-041510-12.

30. Gao M, Craig D, Lequin O, Campbell ID, Vogel V, Schulten K 2003 Structure and functional significance of mechanically unfolded fibronectin type III1 intermediates. Proc Natl Acad Sci USA 100(25):14784-14789.

31. Oberhauser AF, Badilla-Fernandez C, Carrion-Vazquez M, Fernandez JM 2002 The mechanical hierarchies of fibronectin observed with single-molecule AFM. J Mol Biol 319(2):433-447.

32. Ajubi NE, Nijweide PJ, Klein-Nulend J, Burger EH, Semeins CM 1995 Pulsatile fluid flow stimulates nitric oxide (NO) production by osteocytes, but not periosteal fibroblasts. Bone 17(6):566.